International Journal of Impact Engineering, Volume 127, May 2019, pp. 100-109
DOI:10.1016/j.ijimpeng.2019.01.009

A critical study on impact damage simulation of IM7/8552 composite laminate plate

Hao Cui[a,b,1], Daniel Thomson[a], Sina Eskandari[a], Nik Petrinic[a]

[a] *Department of Engineering Science, University of Oxford, Oxford, United Kingdom*

[b] *School of Aerospace, Transport and Manufacturing, Cranfield University, Cranfield, United Kingdom*

Keywords

Composites; Plate impact; Numerical simulation; Modelling

Abstract

Plate impact tests on IM7/8552 composite laminates with different projectile incident angles and velocities were carried out. Numerical simulations were conducted to predict the impact damage, with both Puck and LaRC failure criteria having been employed in this study. The dynamic failure performance of IM7/8552 lamina was reviewed first, by referring to data obtained from experiments conducted at a range of strain rates. The performance of the assessed modelling approaches was evaluated by comparing the results of simulations against experimentally (quantitatively and qualitatively) acquired projectile velocity, impact load and the failure modes of the plates. It proved to be challenging to model

[1]Corresponding author: hao.cui@cranfield.ac.uk

the macroscopic damage of the laminate at elevated projectile velocities; further improvement can be made through enriching the dynamic material data and mitigating the mismatch between the complex fibre architecture and its numerical representation.

1. Introduction

Composite fibre reinforced polymer composites have gained extensive application in aerospace industry [1,2] and other industrial sectors including automotive [3] and civil engineering [4]. These materials have shown superior mechanical performance compared with metallic counterparts, thanks to their high stiffness and strength in the fibre direction. Due to their anisotropic properties and the combination of fibre reinforcement and polymer matrix, their failure modes have been found to be very complicated [5–7]. Many of these composite structures may experience impact damage from different sources [8], such as bird strike on aero-structures [9] and crashing of large vehicles [10]. Analysis and prediction of the failure behaviour under impact loading then become vital in the design and certification of such structures.

A lot of theories have been proposed for predicting the damage of composites, 19 of them have been benchmarked during the World Wide Failure Exercise(WWFE) [11–13]. It was concluded from this exercise that few of the current predictive failure theories were robust enough for industrial applications. Some of these failure theories reflecting on the physical failure mechanisms of composites, such as Puck's failure criteria[14,15], have shown

promising performance in some stress conditions. In recent years, several of these failure criteria have been increasingly employed in predicting damage and fracture of composites, including the dynamic failure process. The low velocity impact damage of composite laminates have been mostly investigated, successful prediction from Puck's theory [16] have been reported. The LaRC model [17] also uses a phenomenological approach to propose a failure criteria specifically for fibre reinforced laminate composites. This model also may take nonlinear matrix shear behaviour into account and it relates laminate configuration to ply thickness and toughness [18], and its performance has been successfully demonstrated [19]. A continuum damage model has been proposed using these failure criteria [20,21]. Nonlinear behaviour due to fibre rotation is also incorporated into the model by [22].

An exhaustive review of dynamic modelling work was not provided due to the scope of the current paper, considering the fact that hundreds of papers per year being published on the composites damage modelling [23]. Despite the increasing volume of failure theories and numerical methodologies, our confidence in our composite modelling capability remains to be confirmed due to the lack of systematic evaluation, such as the round-robin tests from the WWFE [11–13]. It could be relatively easy to match some specific experiments with numerical modelling, for example by tuning some damage parameters. However, it is not conclusive to justify the validity of a modelling method if the input parameters were calibrated against the same set of experiments, which the model is then used to reproduce.

The IM7/8552 has been one of the mostly studied composite material systems so far. Various experiments have been reported on the ultimate strength in the fibre failure and the inter-fibre failure modes, which are important input data for predicting the initiation of damage, as highlighted in the previous WWFE[11–13].. The fracture toughness of different failure modes, critical for analysing the growth and propagation of damage, have also been studied extensively. On top of many studies in the quasi-static domain, it is worth noting that considerable work is also available in dynamic regime. These accumulated data on the IM7/8552 material have made it possible to calibrate strain rate-dependent models for dynamic failure simulation, and arguably, the numerical simulation on this material may represent state of the art capability in predicting dynamic failure of composites in general.

The aim of this paper is to provide a benchmark study on the dynamic damage modelling of composites based on the Puck and LaRC failure criteria, using a bespoke impact test on IM7/8552 composites. This work may help to highlight the performance and drawback of current numerical methods, and provide insight on potential improvement in future. A comprehensive survey of the properties of IM7/8552 laminates is provided as well, for calibrating the material input cards of both models.

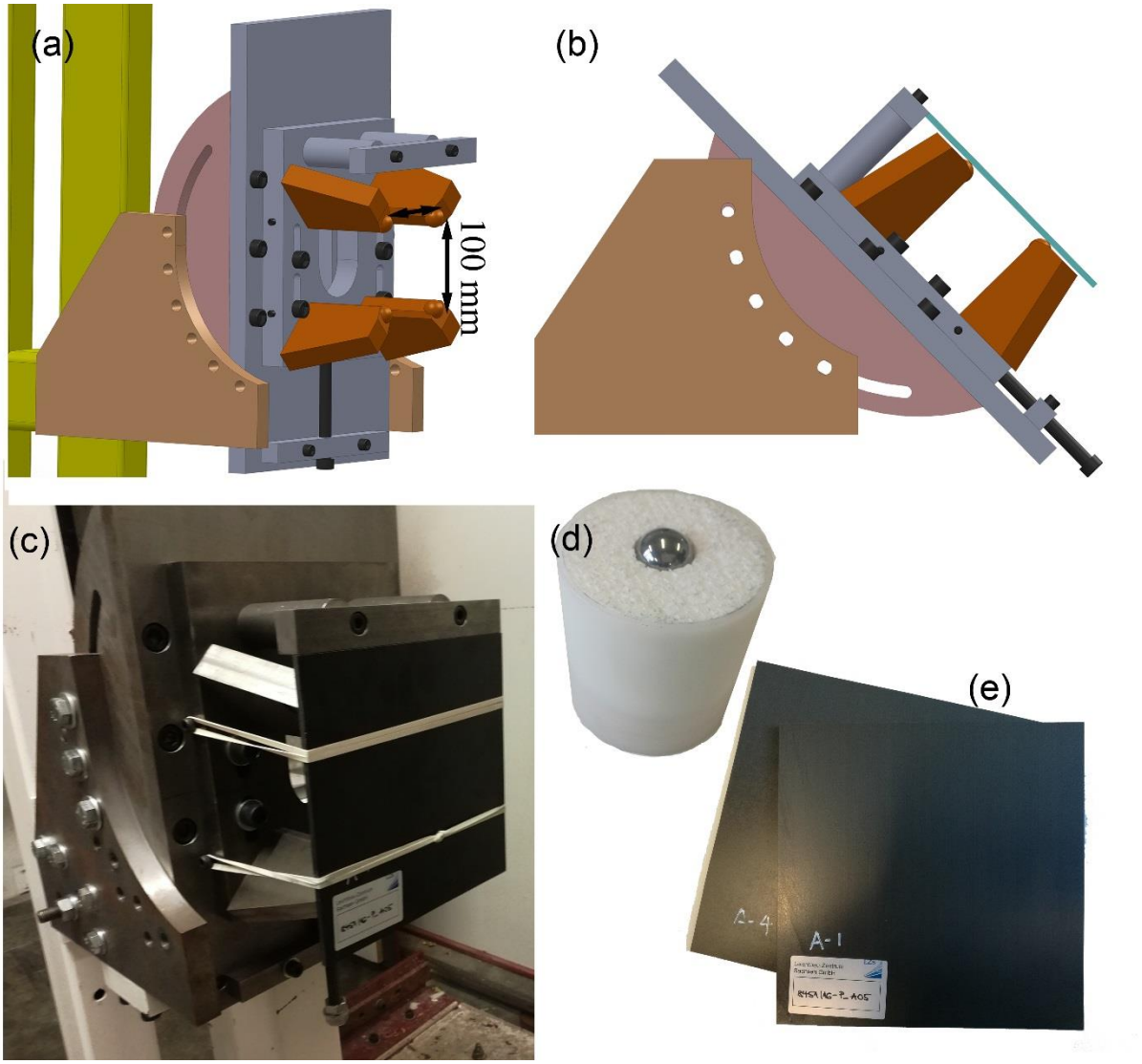

Fig.1 Plate impact setup,(a) the test configuration for 90°impact; (b) the configuration for 45°impact;(c) the actual test fixture with elastic band for holding the plate in place;(d) the projectile(steel ball) in foam sabot; (e) the plate sample

2. Plate impact experiments

2.1 Material and sample

The samples were made with the IM7/8552 unidirectional prepregs, a detailed introduction of the material will be given in Section 3.4. The layup was [0/45/90/-45]5s,

resulting in nominal thickness of 5mm. All panels have been checked with C-Scan to ensure that good quality has been achieved with the manufacturing process, and then cut into the size of 200*200mm using a diamond saw.

2.2 Test setup

The plate impact experiment in this section aims to investigate the failure mode of composite panels under ballistic loading and provide detailed dataset for validating the dynamic failure analysis. As shown in the Fig. 1, the panel was supported with 4 ball bearings of 20 mm diameter. The space between these supporting balls is 100mm. Rubber bands were used to hold the panel on the fixture. The constraint from these rubber bands can be safely ignored due to their low moduli and strength. The fixture and sample holding was designed in such a way that, it is very easy to be accurately simulated in a finite element environment, avoiding complicated boundary conditions from traditional frame supports.

The plates were impacted with steel ball of 20mm diameter, the mass of these projectiles was around 32.7 grams. The projectile was embedded in a foam sabot, and accelerated to the required velocity using a 70 mm gas gun.

The composite plates were impacted at two different angles: 90° normal impact and 45° oblique impact; 10 tests were conducted for each angle. The impact velocity ranged from 21m/s up to 157 m/s, resulting in different combinations of failure modes.

2.3 Data process

A Photron high-speed camera was employed to capture the impact event. The digital image correlation (DIC) method was used to analyse the displacement of the projectiles. The velocity of the projectiles were then analysed from the change of displacement between frames of image. The light curtain attached on the gun also provided the velocity of the projectile, and it has been verified that the difference in velocity estimated between these two methods was less than 5%.

It has been very challenging to record the impact force during these high velocity impact events. In this work, only the displacement and velocity of the projectile was obtained with reasonable accuracy and reliability, using the DIC method. The acceleration of balls were calculated by further differentiation of the velocity history, which is smoothed with moving averaging method. The impact load applied on the plates was the calculated as $F = a\,m$, where a and m are the acceleration and mass of the projectile.

Table 1 Elastic properties for IM7/8552 unidirectional composite

E11	162095.8	Mpa
E11c	140928.9	Mpa
E22c	9721.61	Mpa
G12	4688.436	Mpa
v12	0.362	

3. Dynamic damage theory

For the two compared models, an orthotropic linear elastic behaviour is shared among them, with the elastic properties listed in Table.1. The stiffness of the IM7/8552 is considered as strain rate dependent in the LaRC model. The detailed damage models are introduced as follows.

3.1 Puck failure criteria

For matrix or Inter-fibre fracture (IFF) a modified Puck failure criterion was used [24]. The original Puck criterion [14] is a Mohr-Coulomb based theory where a frictional, or pressure-dependent, failure function, f_E, is evaluated on potential fracture planes transverse to the fibre direction. A numerical search is required in order to determine the critical plane where the failure function, f_E, is maximized. The failure function, or exposure because it indicates the material proximity to failure, is evaluated by rotating the material stress state onto the potential fracture plane (**Error! Reference source not found.**), where the shear stresses, τ_{n1} and τ_{nt}, drive the onset of fracture and the normal stress, σ_n, can either promote or impede this depending, respectively, on if it is tensile or compressive. Because of this, Puck's criterion is given by two equations depending on the direction of the normal stress, σ_n. The surface tractions on the Puck failure plane is calculated as:

129 $$\begin{bmatrix}\sigma_1\\ \sigma_n\\ \sigma_t\\ \tau_{n1}\\ \tau_{nt}\\ \tau_{1t}\end{bmatrix}=\begin{bmatrix}1 & 0 & 0 & 0 & 0 & 0\\ 0 & c^2 & s^2 & 0 & 2sc & 0\\ 0 & c^2 & s^2 & 0 & -2sc & 0\\ 0 & 0 & 0 & c & 0 & s\\ 0 & -cs & cs & 0 & c^2-s^2 & 0\\ 0 & 0 & 0 & -s & 0 & c\end{bmatrix}\cdot\begin{bmatrix}\sigma_{11}\\ \sigma_{22}\\ \sigma_{33}\\ \tau_{12}\\ \tau_{23}\\ \tau_{13}\end{bmatrix} \quad (1)$$

130 where $c = \cos(\theta)$ and $s = \sin(\theta)$.

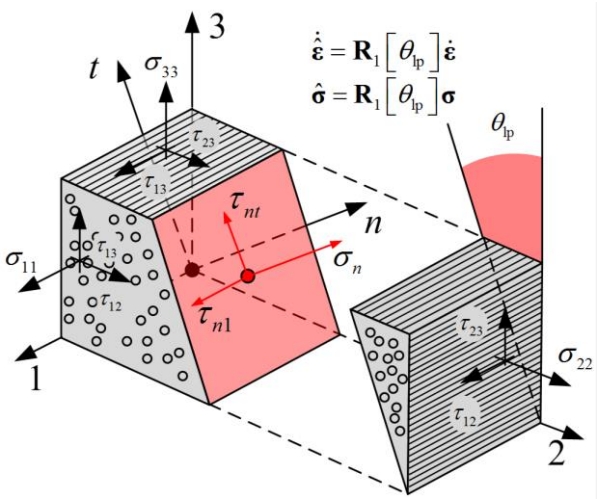

131

132 Fig.2. Schematic view of the rotation performed to transform the stresses into the IFF plane.

133 The stress exposure, f_E, given below, indicates the proximity of the material to IFF-

134 type failure on the considered potential fracture plane with a value ranging from 0, unloaded

135 material, to 1, failure initiation [14,25].

136 $$f_E = \begin{cases}\sqrt{(1-p_t)^2\left(\frac{\sigma_n}{Y_T}\right)^2+\left(\frac{\tau_{n1}}{R_{n1}}\right)^2+\left(\frac{\tau_{nt}}{R_{nt}}\right)^2}+p_t\frac{\sigma_n}{Y_T}\geq 1 \text{ for } \sigma_n\geq 0\\ \sqrt{\left(p_c\frac{\sigma_n}{Y_C}\right)^2+\left(\frac{\tau_{n1}}{R_{n1}}\right)^2+\left(\frac{\tau_{nt}}{R_{nt}}\right)^2}+p_c\frac{\sigma_n}{Y_C}\geq 1 \text{ for } \sigma_n<0\end{cases} \quad (2)$$

137 where p_t, p_c and internal friction parameters [15],$Y_T$is the transverse tensile strength, $Y_C$is

138 the transverse tensile strength. $R_{n1}$is the in-plane shear strength, R_{nt} is calculated as [26]:

$$R_{nt} = Y_C \cos^2 \theta_{fr}^0 \quad (3)$$

where θ_{fr}^0 is the failure angle in transverse compression tests[27].

After failure is predicted using the above criterion, a bilinear cohesive law is used of the type described in [28,29], illustrated in **Error! Reference source not found.**, to damage the tractions on the fracture plane, σ_n, τ_{n1} and τ_{nt}. In tis formulation, a damage variable D is defined to produce linear softening in the effective stress vs effective displacement space, $\sigma_{eff} - \delta$, from the point of initiation, δ_0, to final failure, δ_C:

$$D = \max\left\{0, \min\left\{1, \frac{\delta_C(\delta - \delta_0)}{\delta(\delta_C - \delta_0)}\right\}\right\} \quad (4)$$

With the effective displacements, δ, obtained from the effective strain and characteristic element length, l_c, introduced to alleviate the mesh dependency problem of continuum damage modelling [18,19]:

$$\delta = l_c \varepsilon_{eff} \quad (5)$$

and the displacement at failure calculated from the mixed mode fracture toughness, G_T:

$$\delta_C = \frac{2G_T}{\sigma_{eff}^C} \quad (6)$$

$$G_T = \begin{cases} \frac{G_{IC}G_{IIC}(1+\eta^2\lambda)}{G_{IIC}+G_{IC}\eta^2\lambda}, & \gamma_{eff} \neq 0 \\ G_{IIC}, & \gamma_{eff} = 0 \end{cases} \quad (7)$$

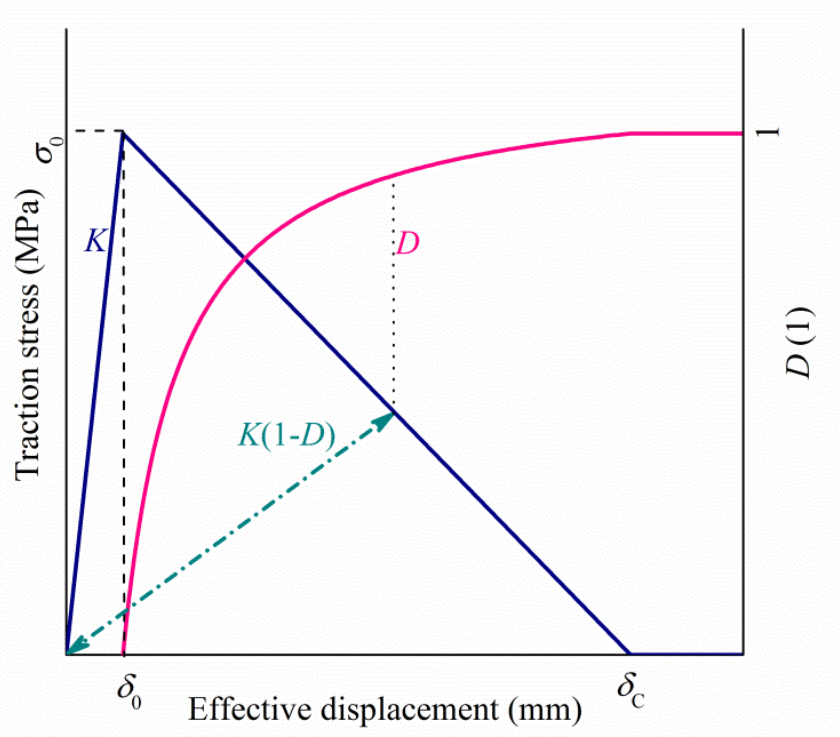

Fig.3. Damage evolution at Puck failure plane

The material may fail in the fibre direction under tension and compression load, which is predicted here by maximum stress criteria. The continuum stiffness degradation will start once the failure criteria is satisfied, which is controlled in a similar way as shown in Fig.3, where the fibre fracture toughness equal to the area under the damage evolution curve.

Finally, fully-damaged elements, identified by the damage variable for any of the failure modes reaching a limit of 0.999, are deleted to avoid numerical instabilities and allow full perforation of the plate.

3.2 LaRC failure criteria and Maimi damage model

The LaRC is a set of six phenomenological failure criteria with the assumption of plane stress conditions. LaRC uses *in situ* strength for evaluation of failure which depends on where the ply is situated in the laminate, the number of plies bundled together, and the orientation of the fibers in outer plies. *In situ* properties are calculated based on crack propagation in a constrained ply. LaRC criterion for matrix failure under transverse tension reads:

$$(1-g)\frac{\sigma_{22}}{Y_{T,is}} + g(\frac{\sigma_{22}}{Y_{T,is}})^2 + g(\frac{\tau_{12}}{R_{12,is}})^2 \leq 1 \quad (8)$$

Where $g = \frac{G_{IC}}{G_{IIC}}$ and "*is*" subscript represents *in situ* property. The criterion for matrix failure under compression is:

$$(\frac{\tau_{eff}}{R_{nt}})^2 + \mathrm{g}(\frac{\tau_{eff}}{R_{n1,is}})^2 \leq 1 \quad (9)$$

Where the subscript "*eff*" means the stress components acting in fracture plane which is calculated according to Eq(1). The transverse shear strength R_{nt} for LaRC model is calculated as:

$$R_{nt} = Y_C \cos(\theta_{fr}^0)\left[\sin(\theta_{fr}^0) + \frac{cos(\theta_{fr}^0)}{tan(2\theta_{fr}^0)}\right] \quad (10)$$

For failure in fibre compression, the initial misalignment in the fibres is calculated and, based on that, the effective stresses are derived. The effective stresses then contribute to Mohr-Coulomb criterion, where, in the presence of compressive transverse loading, it reads:

$$\langle \frac{|\tau_{12}^{m}| + \eta^{L}\sigma_{22}^{m}}{R_{n1,is}} \rangle \leq 1 \quad (11)$$

And in the presence of tensile and transverse loading, the LaRC criterion reads:

$$(1-g)\frac{\sigma_{22}^{m}}{Y_{T,is}} + \mathrm{g}(\frac{\sigma_{22}^{m}}{Y_{T,is}})^2 + \mathrm{g}(\frac{\tau_{12}^{m}}{R_{12,is}})^2 \leq 1 \quad (12)$$

In Eq (11, 12), the superscript "m" means the stress in the local coordinate with consideration of fibre misalignment. Detailed information can be found in [18]. The maximum stress criteria have been used for fibre tension failure prediction, similar to the previous Puck model.

The damage evolution is triggered once any failure criterion is reached, and the degradation of stiffness is determined based on the energy dissipation per volume, similar to what was introduced in previous section. All of damage parameters are scalar and evolve linearly, but the damage parameter in fibre direction which evolves exponentially after fibre pull-out. The details of the model is discussed in [21] and [30]. Element erosion is applied to prevent instability. This criterion deletes an element when any damage variable reaches 0.999.

3.3 Numerical plate impact model

A numerical model has been built to simulate the plate impact experiments in Ls-Dyna environment. The plate was modelled with 3 dimensional solid elements as shown in Fig.4. The element size was 1x1x0.125 mm^3, one element per ply through-thickness. This paper aims to evaluate the performance of these numerical models with the given mesh size.

It is expected that simulation accuracy will improve with finer mesh, however, it may be less practical for industrial application. Two different user subroutines have been prepared accordingly for both of the damage theories introduced in Section 2, representing the elastic deformation and damage of the IM7/8552 laminates. The delamination is considered as a special case of inter-fibre failure, and is simulated here with Puck and LaRC in bulk elements. The supports and projectile were modelled as rigid bodies with a 3D solid mesh of approximately 2mm in length.

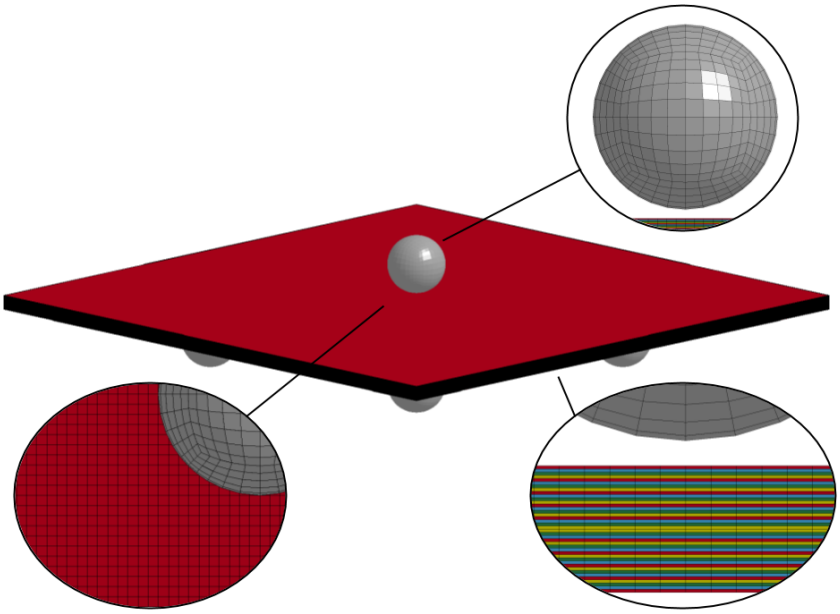

Fig.4. Simple 200x200x40 element mesh of the impacted plate, one element per ply through-thickness, with supports and projectile modelled as rigid solids.

3.4 Rate-dependent mechanical properties of IM7/8552

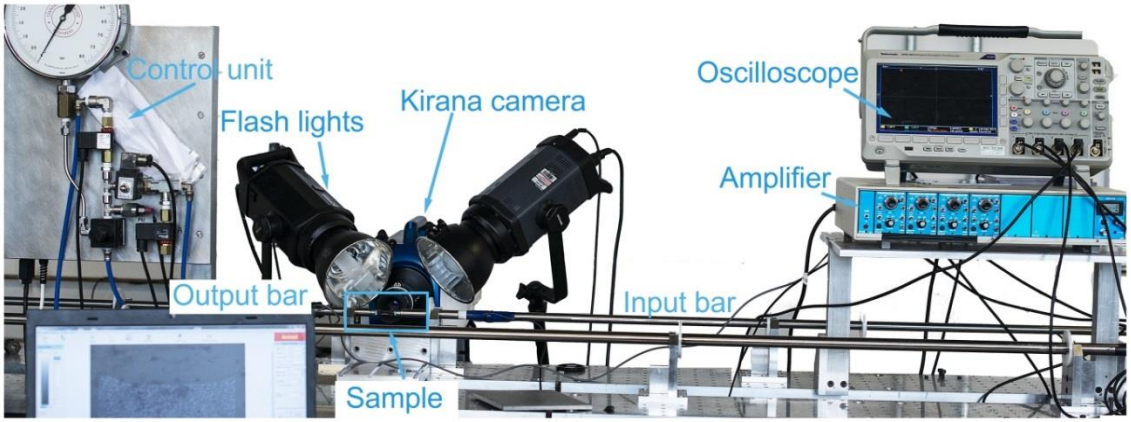

Fig.5. Split Hopkinson bar test system

The IM7/8552 material has been characterized at different strain rates with various combinations of stress conditions, including considerable dynamic studies using the split Hopkinson bar test system, one example for which is shown in Fig.4. The material characterization will not be introduced in this work, instead detailed information of some experiments can be found in recent publications of the authors[24,31–33]. These experiments, in combination with work from peers [34–37], resulted in an relatively complete datasheet representing the rate-dependent failure envelope of IM7/8552 laminate. A summary of all material data used in this simulation has been presented in Table.2.

Table.2 Summary of IM7/8552 strength and fracture toughness data

Property	Value	Test configuration	Strain rate	References
S_{11}**(tension)**	2625 MPa	Uniaxial tension	QS	[38]
S_{11}**(Compression)**	1451 MPa	Uniaxial compression	4e-4 s^{-1}	[34]
S_{11}**(Compression)**	2008 MPa	Uniaxial compression	119 s^{-1}	[34]
S_{22}**(Tension)**	60.2 MPa	Uniaxial tension	1e-4 s^{-1}	[39]

S_{22}**(Tension)**	113.3 MPa	Uniaxial tension	300 s^{-1}	[39]
S_{22}**(Compression)**	400.6 MPa	Uniaxial compression	5e-4 s^{-1}	[32]
S_{22}**(Compression)**	248.7 MPa	Uniaxial compression	300 s^{-1}	[39]
S_{12}	112.7 MPa	±45° laminates tension	5e-4 s^{-1}	[31]
S_{12}	149.7 MPa	±45° laminates tension	1300 s^{-1}	[31]
G_{IC}	0.22 N/mm	Double cantilever beam	Quasi-static	[40]
GIC	0.2 N/mm	Dynamic wedge opened double cantilever beam	Dynamic	[41]
G_{IIC}	0.66 N/mm	End notched flexure	Quasi-static	[42]
G_{IIC}	0.922 N/mm	End notched flexure	Dynamic	[42]
G_{FT}	82.0 N/mm	Compact tension	Quasi-static	[33]
G_{FT}	195.8 N/mm	Compact tension	Dynamic	[33]
G_{FC}	101.6 N/mm	Compact compression	Quasi-static	[43]
G_{FC}	165.6 N/mm	Compact compression	Dynamic	[43]

Here S11 is the longitudinal strength, S22 is the transverse strength, S12 is the in-plane shear strength. GIC is the mode I delamination fracture toughness, GIIC is the mode II delamination fracture toughness, GFT is the fracture toughness in fibre tension mode, G_{FC} is the fracture toughness in fibre compression mode

The longitudinal tensile strength, obtained from tension tests of the 0° plate, has recently been reported to be dependent on the through-thickness compression stress[44] but this effect was not taken into consideration. In addition, diverse data has been observed in the longitudinal compression strength and there could be more than 50% difference in the strength measured, depending on the specimen geometry and test methods [36,45,46]. The transverse tension strength is also very difficult to measure, as it could be largely affected by surface treatment and boundary conditions [43], and the data reported in this paper is lower than data available in literature [43,47]. The mode I delamination fracture toughness is fairly

constant across thr literature, however, the mode II delamination toughness shows significant variation [48], and could also be dependent on the transverse stress [49]. Finally, fracture toughness tests in the fibre failure mode are limited and pioneering work from Pinho et.al [50] suggest 20% difference in the fracture toughness from the value listed in above.

In the simulation with Puck's failure criteria, the material input card was filled with those parameters tested at high strain rate wherever available. In the LaRC damage model, a rate-dependent model has been introduced for representing the gradual change of material parameters with respect to the strain rate of each individual element. There is a limit of $300s^{-1}$ for strain rate for stability after which the parameters will not vary anymoreIn addition to strain-rate damping. These viscoelastic parameters are obtained based on experiments by [51]. Elastic properties are calculated based on:

$$f_e(\dot{\varepsilon}) = (k_e\dot{\varepsilon})^{\frac{1}{n_e}},\ k_e = 1.60 \times 10^{-4}, n_e = 2 \tag{11}$$

Strength properties are also updated with local strain rate:

$$f_e(\dot{\varepsilon}) = (k_u\dot{\varepsilon})^{\frac{1}{n_u}}, k_u = 1.13 \times 10^{-4}, n_u = 4 \tag{12}$$

4. Results from experiments and simulations

There were 20 experiments on the composite plates at velocities ranged from 20m/s to 157 m/s. It has been observed that matrix dominated failure including delamination is the major failure mode in low and medium velocity impact; more fibre rupture and splitting was

noticed as the increase of impact velocity. Therefore, four testing cases have been simulated in the paper for a comprehensive evaluation of these numerical models in capturing different failure modes Each of the testing case is introduced in a separate section as following.

4.1 90 degree impact at 59m/s

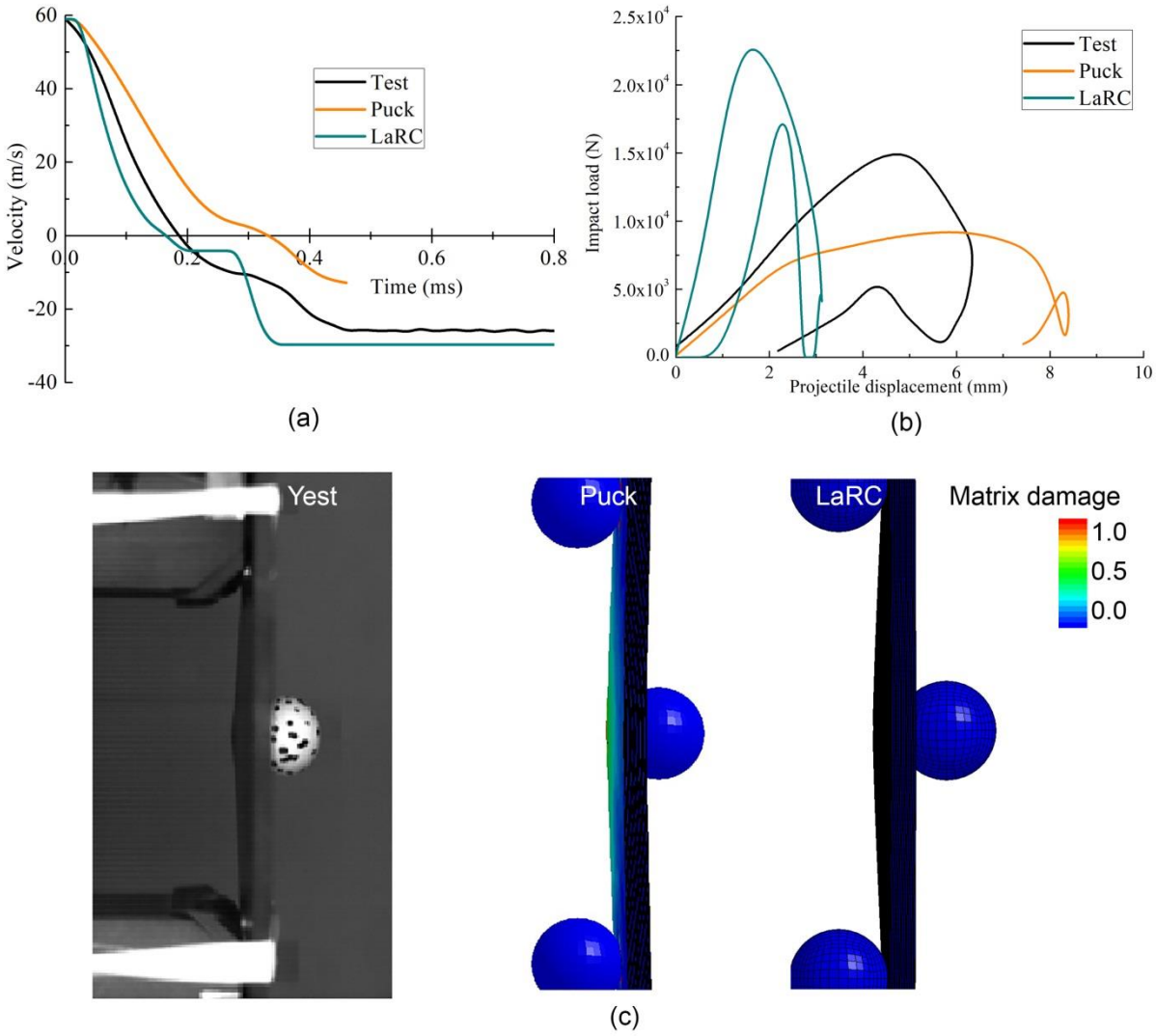

Fig.6 90° plate impact response at velocity of 59m/s from experiment and simulations: (a) the velocity history during impact; (b) the Impact load-projectile displacement curves(c) comparison of failure modes.

256 The plate tested at 90° with projectile of 59 m/s has been selected for modelling. The
257 global deformation and failure modes from simulations and experiments look very similar
258 among each other as shown in Fig.6c. At this level of impact velocity, matrix dominated inter-
259 fibre failure, including delamination, has been the major failure mode, although not clearly
260 visible from the high-speed camera image here. The deformation of plates have been
261 successfully captured in both Puck and LaRC model.

262 The projectile velocity from simulations and test has been summarized in Fig.6a,
263 where the velocity value changed from positive to negative due to the bouncing back of the
264 projectile. The simulation with Puck didn't capture the full impact event, due to excessive
265 distortion of damaged element that killed the time increment. The LaRC model provided good
266 prediction of the velocity history, the plateau during bouncing back process was due to the
267 vibration of plate that makes it lose contact with projectile, a similar step on experimental
268 curve is also noticeable.

269 The impact load from simulations have been calculated by the acceleration data of
270 projectile, and plotted with experimental results in Fig.6b. The Puck model underestimated
271 the peak contact load during, and the maximum displacement from this simulation was longer
272 than experimental data. The LaRC seemed to overestimate the peak force, and the raising
273 edge of the force-displacement curve is steeper than the other two. The strain rate dependent
274 modulus of LaRC model should be responsible for the artificially increase stiffness of the plate.

4.2 45 degree impact at 55m/s

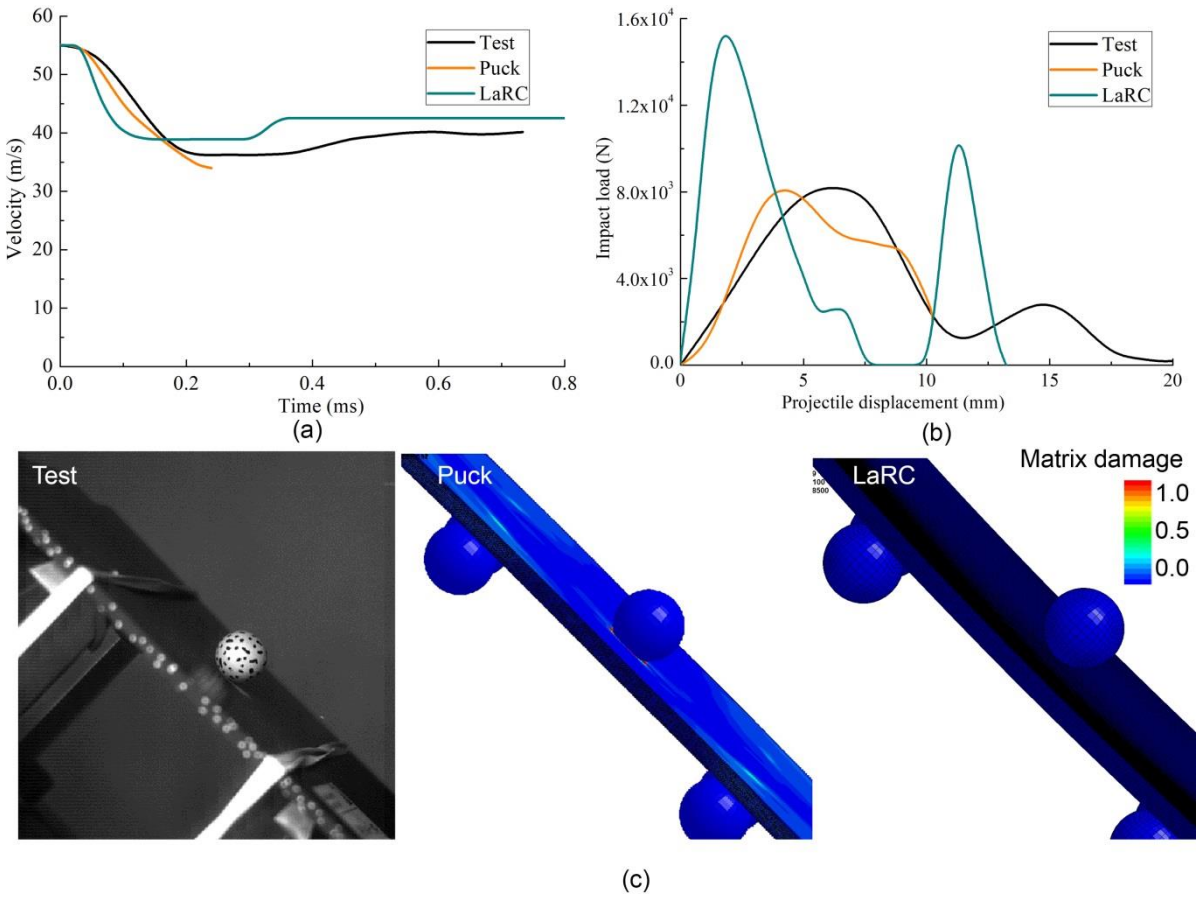

Fig.7 45° plate impact response at velocity of 55m/s from experiment and simulations: (a) the velocity history during impact; (b) the Impact load-projectile displacement curves(c) comparison of failure modes.

The result from plate impact at 45° with projectile velocity of 55m/s is shown in Fig.7. The Puck modelling was terminated after the project lose contract with plate, as element distortion have resulted in significantly reduction of time increment in these simulations. There is not much visible damage from the surface of plate as suggested by Fig.7c. all simulations have reproduced such failure mode, however, the damage index near supporting balls suggests that inter-fibre damage is likely to happen at these four corners as well. The

velocity profiles from both simulations and the experiments agree with each other quite well, indicated that the energy dissipation was also of similar level among them. The Impact load has been nicely reproduced by Puck model, however, the LaRC model have predicted much higher peak load than experimental data.

4.3 90 degree impact at 106 m/s

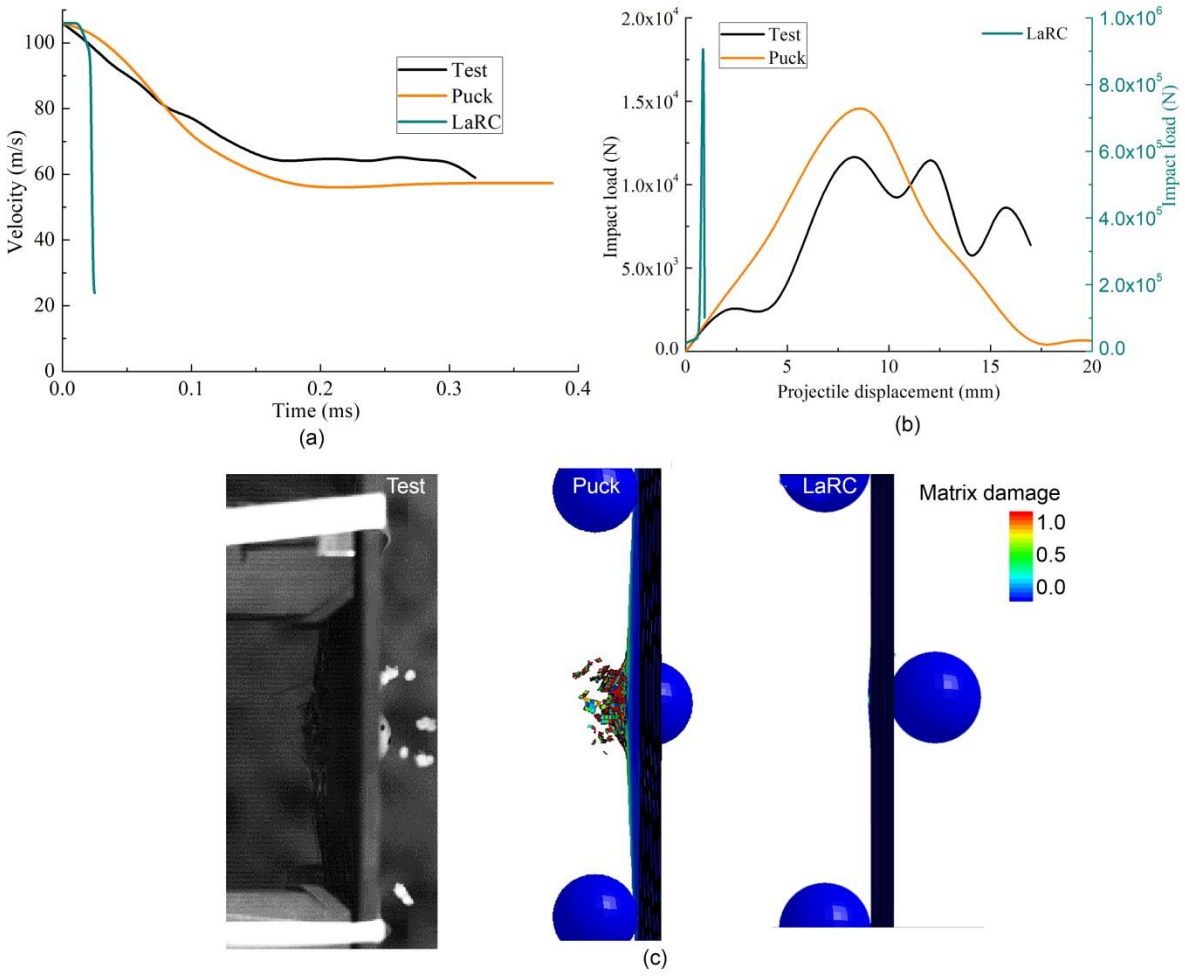

Fig.8 90° plate impact response at velocity of 106m/s from experiment and simulations: (a) the velocity history during impact; (b) the Impact load-projectile displacement curves (c) comparison of failure modes.

There is more damage occurring as the increase of impact velocity, as shown in Fig.8c, and the plate has been penetrated with the projectile in test, with considerable fibre splitting and rupturing. Such failure mode was captured by the Puck failure model, although the damage is largely in the format of fragmentation, rather than the splitting of continuum fibres in test. The velocity of projectile was properly predicted with the Puck model, while LaRC model resulted in very rapid decrease of velocity as shown in Fig.8a. This rapid decrease was correlated to the unusually high impact load as shown in Fig.8b.

4.4 45 degree impact at 106m/s

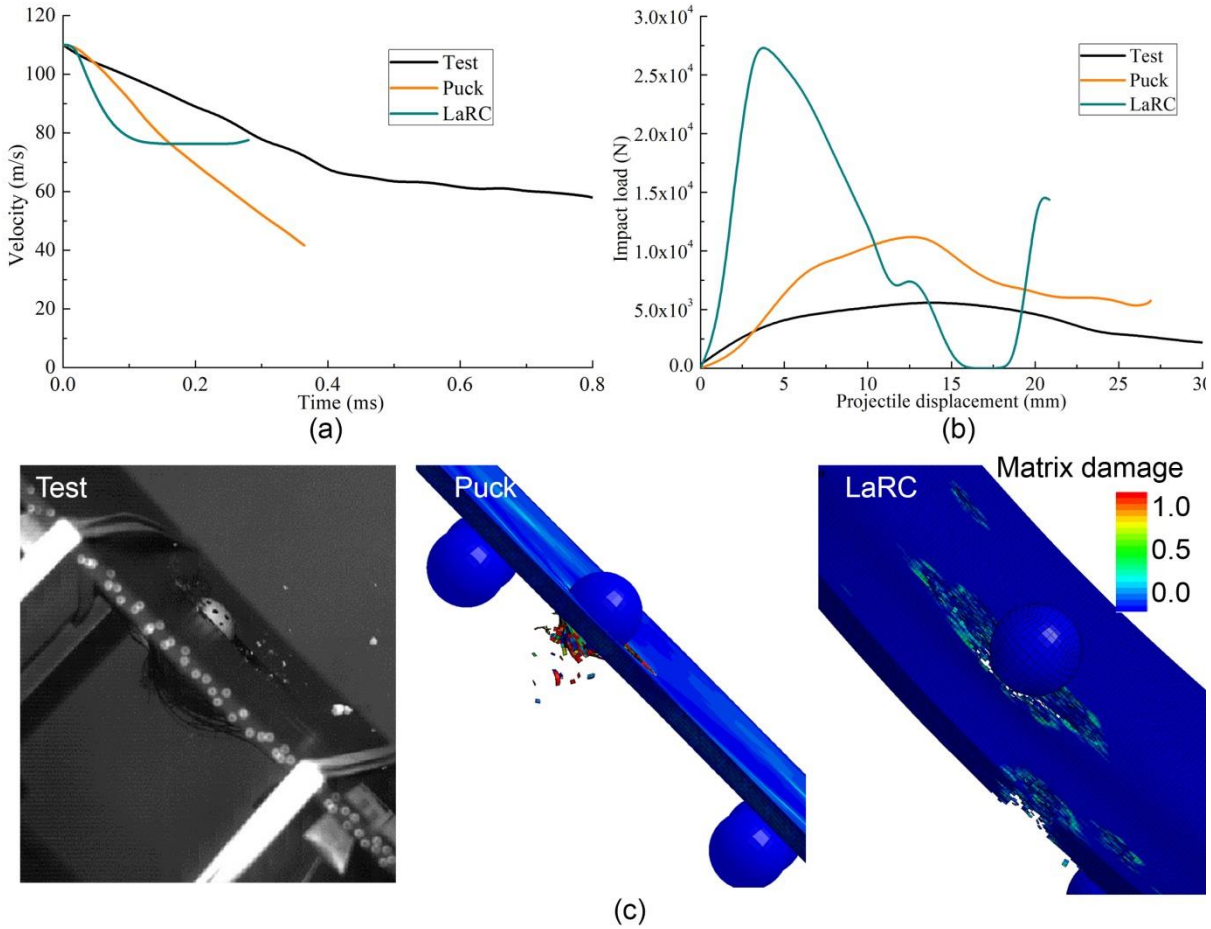

Fig.9 45° plate impact response at velocity of 110m/s from experiment and simulations: (a) the velocity history during impact; (b) the Impact load-projectile displacement curves;(c) comparison of failure modes.

The comparison between experiment and simulation of 45° plate impacted at 110m/s is shown in Fig.9. The penetration damage to plate has been successfully predicted by both models. The Puck model seemed to provide better match with experiment than the LaRC model, as excessive element deletion was noticed from the later one. The velocity history from both simulations show noticeable deviation from the test result. Both models also overestimated the impact load as well.

4.5 Energy absorption

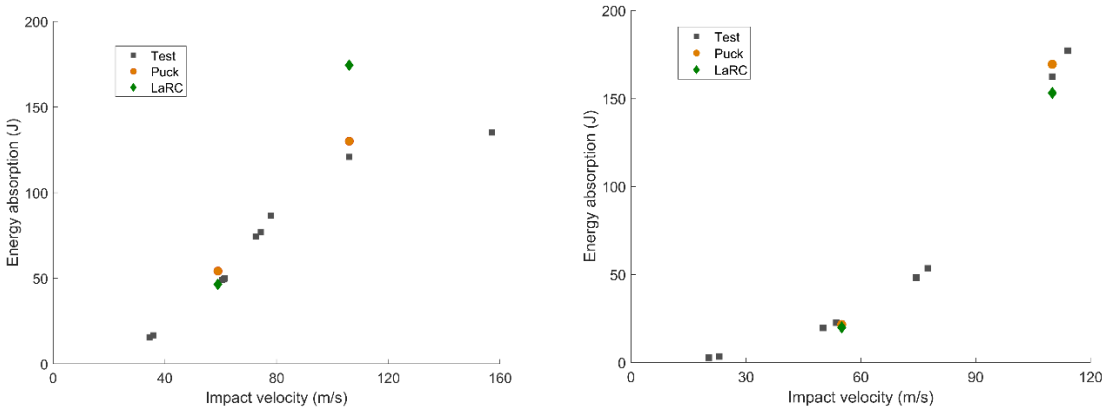

Fig.10. Energy dissipation from experiments and simulations,(a) 90°impact and (b)45°impact

The energy being absorbed during the impact damage of the plate was calculated by the difference of projectile kinetic energy before and after the event. There was rigid movement and vibration of plates excited during the event that also consumed some of the

projectile kinetic energy, therefore, the energy absorption shown in Fig.10a is higher than actual energy dissipated during damage process. In the 90° impact tests, the energy absorption increased with the projectile velocity, which then plateaued due to the penetration of plate. In the 45° impact, the energy absorbed by plate kept increasing within the tested range of velocity. The simulations from both models have reproduced the energy dissipation performance reasonably well.

5. Discussions

An effort has been made here for benchmarking the dynamic modelling capacities on some popular numerical models. It is worth emphasising that, this study shouldn't indicate the level of accuracy of each damage theory, i.e. Puck and LaRC. Rather, this shows the performance of the complete dynamic simulation settings, including also the way of interpreting rate-dependent material data, mass scaling and element erosion etc. Each single setting listed above can have predominant effect on the simulation. In addition, these models were both calibrated with coupon scale tests at two different strain-rate regions (dynamic and quasi-static) and then used directly to model the experiments at the component scale and a range of different impact velocities with no further calibration or fitting of the input parameters. This served to demonstrate a reliable validation of composite modelling capabilities without re-calibration and curve fitting, which has been standard practice in the

337 past. A collection of benchmark tests at different velocities and impact angles, such as the
338 ones presented here, will be critical to validate any developments in this area.

339 The discussion that follows is meant to evaluate the performance of current
340 modelling capabilities, which can be fitted to produce good results for a specific test but found
341 challenging to reproduce a broader range of loading scenarios.

342 For the Puck model, the high strain-rate material data was used and, overall,
343 performed reasonably well in current study, with the impact load and energy dissipation
344 being reproduced with acceptable accuracy. In the LaRC model, on the other hand, both the
345 stiffness and strength were considered as strain rate dependent. However, without tuning
346 these rate-dependent coefficients, the stiffness and peak impact load were overestimated.
347 Technically, rate-dependent material data should be more versatile for modelling dynamic
348 damage process, as the local strain rate keeps changing and is different from one location to
349 another. However, proper calibration of this effect, so as to get a reliable estimation of strain
350 rate for each element, can be very challenging without additional curve fitting to match the
351 experimental result and avoid any overshoots as shown in this work.

352 Another issue observed during this exercise had to do with numerical instabilities
353 due to distortion and failure. Elements may get distorted once the stiffness degradation was
354 triggered by reaching certain failure criteria. Such distortion is highly likely for the inter-fibre

355 failure of Puck theory, which may result in an inclined failure plane in the element with an
356 angle against the loading axis. The distorted elements will reduce the computational time
357 increment, and eventually result in abortion of the simulation, as shown in some of the Puck
358 simulations. Mass scaling can mitigate this issue to some extent, however, its effect is limited
359 as extensive application can artificially increase the whole mass of the model and affect the
360 accuracy of simulation. Similarly, erosion of distorted element may also resulted in lower
361 model mass than reality and severely affect the contact force in the simulation, as was
362 observed for the Puck model at lower velocity impacts in particular.

363 The failure of the plate at medium rate impact was dominated by inter-fibre failure,
364 including delamination. Although cohesive element has been traditionally used for
365 delamination prediction, the Puck and LaRC models that account for general inter-fibre failure,
366 appear to be successful for such simulations. Considering the fact that interface elements
367 normally require high computational effort, continuum damage models with inter-fibre
368 damage within the bulk element can be an efficient alternative solution, especially for
369 engineering applications.

370 The 45° impact test proves extremely useful validation case as it adds complexity to
371 delamination and ply failure with respect to the 90deg impact case. As seen in the numerical
372 results, one same model can produce reasonably good results in the simpler 90° case but fail
373 to match the 45° impact. In addition, in industrial applications impact is unlikely to occur

perfectly normal to a flat plate, instead being more likely to occur on oblique or curved components. The normal velocity to the plate surface in this case, around 78 m/s, was close to the ballistic limit, which makes it significantly more challenging to model. Because of this, a minor under- or overestimation of material properties can result full, partial, or even no perforation, as observed with the difference between the two models compared in section 4.4 – the LaRC based model over-predicted the extent of damage while in the Puck-based model it was under-predicted.

In general, as expected, the numerical models have shown successful prediction of certain test cases, while, failing to match the experiments in others. The velocity history has been found to be relatively easy to reproduce among those experimental data acquired, while the impact load can be very challenging to predict. The complicated plate perforation damage wasn't successfully simulated, probably because of the continuous fibre architecture that cannot be represented by current continuum bulk element. For example, the in-plane shear normally results in splitting of fibres, while there is no distinction between it and the transverse shear rupture of fibres. Novel numerical modelling methodologies are needed to physically represent the microstructures of composites and its corresponding anisotropic failure modes.

A comprehensive understanding of the dynamic damage mechanisms of composites and their evolution with changes in strain-rate will help to provide accurate input data for the

numerical modelling. The IM7/8552 material was one of the most investigated materials, with all dynamic data summarized in Table.2. However, there is still many data missing at dynamic rates, and more experiments in this field are certainly encouraged, as a properly calibrated rate-dependent model of the material properties is key to enhance dynamic modelling capabilities in the future.

6. Conclusions

Plate impact tests have been carried out at two different incidence angles with projectiles of various velocities. The IM7/8552 material was used for making these plates, and the literature survey have been done for its dynamic failure properties.

Numerical models have been developed for predicting the impact damage, where Puck and LaRC failure criteria have been implemented separately for the inter-fibre failure damage.

These models have been successfully used in the past to reproduce coupon-level experiments at certain strain rates, however a proper rate-dependent validation at larger scales has proven challenging without further tuning of material parameters.

The comparison between numerical simulation and experiments showed that, projectile velocity is relatively easy to predict, while the force-displacement curves are challenging to reproduce. There is also deviation between the actual failure modes and

411 numerical prediction, largely due to the mismatch between the complex fibre architecture
412 and its numerical representation.

413 Comprehensive characterization of the material response at dynamic loading rate
414 will contribute to improved dynamic modelling capabilities and avoid the need for curve
415 fitting in order to produce accurate large scale dynamic results.

416 # References

417 [1] GE tests GE9X composite fan blades, Reinf. Plast. (2014) 5. doi:10.1016/S0034-
418 3617(13)70162-0.

419 [2] M. Nishikawa, K. Hemmi, N. Takeda, Finite-element simulation for modeling composite
420 plates subjected to soft-body, high-velocity impact for application to bird-strike
421 problem of composite fan blades, Compos. Struct. 93 (2011) 1416–1423.
422 doi:10.1016/j.compstruct.2010.11.012.

423 [3] P. Feraboli, A. Masini, Development of carbon / epoxy structural components for a high
424 performance vehicle, Compos. Part B. 35 (2004) 323–330.
425 doi:10.1016/j.compositesb.2003.11.010.

426 [4] J.G. Teng, T. Yu, D. Fernando, Strengthening of steel structures with fiber-reinforced
427 polymer composites, J. Constr. Steel Res. Rev. 78 (2012) 131–143.
428 doi:10.1016/j.jcsr.2012.06.011.

[5] A.E. Scott, M. Mavrogordato, P. Wright, I. Sinclair, S.M. Spearing, In situ fibre fracture measurement in carbon – epoxy laminates using high resolution computed tomography, Compos. Sci. Technol. 71 (2011) 1471–1477. doi:10.1016/j.compscitech.2011.06.004.

[6] S.C. Garcea, I. Sinclair, S.M. Spearing, P.J. Withers, Mapping fibre failure in situ in carbon fibre reinforced polymers by fast synchrotron X-ray computed tomography, Compos. Sci. Technol. 149 (2018) 81–89. doi:10.1016/j.compscitech.2017.06.006.

[7] A.E. Scott, I. Sinclair, S.M. Spearing, A. Thionnet, A.R. Bunsell, Composites : Part A Damage accumulation in a carbon / epoxy composite : Comparison between a multiscale model and computed tomography experimental results, Compos. Part A. 43 (2012) 1514–1522. doi:10.1016/j.compositesa.2012.03.011.

[8] S. Abrate, Impact on Laminated Composite Materials, Appl Mech Rev. 44 (1991) 155–190.

[9] S. Georgiadis, A.J. Gunnion, R.S. Thomson, B.K. Cartwright, Bird-strike simulation for certification of the Boeing 787 composite moveable trailing edge, Compos. Struct. 86 (2008) 258–268. doi:10.1016/j.compstruct.2008.03.025.

[10] G. Savage, I. Bomphray, M. Oxley, Exploiting the fracture properties of carbon fibre composites to design lightweight energy absorbing structures, 11 (2004) 677–694.

447 doi:10.1016/j.engfailanal.2004.01.001.

448 [11] P.D. Soden, A.S. Kaddour, M.J. Hinton, Recommendations for designers and
449 researchers resulting from the world-wide failure exercise, Compos. Sci. Technol. 64
450 (2004) 589–604. doi:10.1016/s0266-3538(03)00228-8.

451 [12] M. Hinton, Failure Criteria in Fibre Reinforced Polymer Composites: Can any of the
452 Predictive Theories be Trusted, in: NAFEMS World Congr., Boston, 2011: p. 66.

453 [13] A. Kaddour, M. Hinton, Benchmarking of triaxial failure criteria for composite
454 laminates: Comparison between models of 'Part (A)' of 'WWFE-II,' 2012.
455 doi:10.1177/0021998312449887.

456 [14] A. Puck, H. Schurmann, Failure analysis of FRP laminates by means of physically based
457 phenomenological models, Compos. Sci. Technol. 58 (2002) 30.

458 [15] A. Puck, J. Kopp, M. Knops, Guidelines for the determination of the parameters in
459 Puck's action plane strength criterion, Compos. Sci. Technol. 62 (2002) 8.

460 [16] Y. Shi, C. Pinna, C. Soutis, Modelling impact damage in composite laminates: A
461 simulation of intra- and inter-laminar cracking, Compos. Struct. 114 (2014) 10–19.
462 doi:10.1016/j.compstruct.2014.03.052.

463 [17] C.G. Dávila, P.P. Camanho, C.A. Rose, Failure criteria for FRP laminates, J. Compos.

Mater. 39 (2005) 323–345. doi:10.1177/0021998305046452.

[18] P.P. Camanho, C.G. Dávila, S.T. Pinho, L. Iannucci, P. Robinson, Prediction of in situ strengths and matrix cracking in composites under transverse tension and in-plane shear, Compos. Part A Appl. Sci. Manuf. 37 (2006) 165–176. doi:10.1016/j.compositesa.2005.04.023.

[19] S.T. Pinho, C.G. Dávila, P.P. Camanho, L. Iannucci, P. Robinson, Failure Models and Criteria for FRP Under In-Plane or Three-Dimensional Stress States Including Shear Non-linearity, Nasa/Tm-2005-213530. (2005) 68. doi:NASA/TM-2005-213530.

[20] H. Ghiasi, D. Pasini, L. Lessard, Optimum stacking sequence design of composite materials Part I: Constant stiffness design, Compos. Struct. (2009). doi:10.1016/j.compstruct.2009.01.006.

[21] P. Maimí, P.P. Camanho, J.A. Mayugo, C.G. Dávila, A continuum damage model for composite laminates: Part II – Computational implementation and validation, Mech. Mater. 39 (2007) 909–919. doi:10.1016/j.mechmat.2007.03.006.

[22] S. Eskandari, F.M. Andrade Pires, P.P. Camanho, A.T. Marques, Intralaminar damage in polymer composites in the presence of finite fiber rotation: Part II – Numerical analysis and validation, Compos. Struct. 151 (2016) 127–141. doi:10.1016/j.compstruct.2016.01.048.

[23] Scopus - Document search results on the composites damage modelling, last visited on 15th Oct, 2018, Https://Www.Scopus.Com. (2018).

[24] D.M. Thomson, H. Cui, B. Erice, J. Hoffmann, J. Wiegand, N. Petrinic, Experimental and numerical study of strain-rate effects on the IFF fracture angle using a new efficient implementation of Puck's criterion, Compos. Struct. 181 (2017) 325–335. doi:10.1016/j.compstruct.2017.08.084.

[25] A. Puck, J. Kopp, M. Knops, Guidelines for the determination of the parameters in Puck's action plane strength criterion, Compos. Sci. Technol. 62 (2002) 371–378. doi:10.1016/S0266-3538(01)00202-0.

[26] J. Wiegand, Constitutive modelling of composite materials under impact loading, PhD thesis (2008).

[27] J. Wiegand, N. Petrinic, B. Elliott, An algorithm for determination of the fracture angle for the three-dimensional Puck matrix failure criterion for UD composites, Compos. Sci. Technol. 68 (2008) 2511–2517. doi:10.1016/j.compscitech.2008.05.004.

[28] S.T. Pinho, L. Iannucci, P. Robinson, Physically based failure models and criteria for laminated fibre-reinforced composites with emphasis on fibre kinking. Part II: FE implementation, Compos. Part A Appl. Sci. Manuf. 37 (2006) 766–777. doi:10.1016/j.compositesa.2005.06.008.

500 [29] P.P. Camanho, Failure Criteria for Fibre-Reinforced Polymer Composites, Demegi, Feup.
501 (2002) 1–13.

502 [30] P. Maimí, D. Trias, E. V González, J. Renart, Nominal strength of quasi-brittle open hole
503 specimens, Compos. Sci. Technol. 72 (2012) 1203–1208.
504 doi:10.1016/j.compscitech.2012.04.004.

505 [31] H. Cui, D. Thomson, A. Pellegrino, J. Wiegand, N. Petrinic, Effect of strain rate and fibre
506 rotation on the in-plane shear response of ±45° laminates in tension and compression
507 tests, Compos. Sci. Technol. 135 (2016) 106–115.
508 doi:10.1016/j.compscitech.2016.09.016.

509 [32] H. Cui, A.R. Melro, M. Yasaee, Inter-fibre failure of through-thickness reinforced
510 laminates in combined transverse compression and shear load, Compos. Sci. Technol.
511 165 (2018) 48–57. doi:10.1016/j.compscitech.2018.06.011.

512 [33] J. Hoffmann, H. Cui, N. Petrinic, Determination of the strain-energy release rate of a
513 composite laminate under high-rate tensile deformation in fibre direction, Compos. Sci.
514 Technol. 164 (2018) 110–119. doi:10.1016/j.compscitech.2018.05.034.

515 [34] M. Ploeckl, P. Kuhn, J. Grosser, M. Wolfahrt, H. Koerber, A dynamic test methodology
516 for analyzing the strain-rate effect on the longitudinal compressive behavior of fiber-
517 reinforced composites, Compos. Struct. 180 (2017) 429–438.

518 doi:10.1016/j.compstruct.2017.08.048.

519 [35] M.W. Czabaj, J.G. Ratcliffe, Comparison of intralaminar and interlaminar mode-I
520 fracture toughness of unidirectional IM7/8552 graphite/epoxy composite, NASA Tech.
521 Rep. (2012) 1–18. doi:https://doi.org/10.1016/j.compscitech.2013.09.008.

522 [36] H. Koerber, P.P. Camanho, High strain rate characterisation of unidirectional carbon–
523 epoxy IM7-8552 in longitudinal compression, Compos. Part A Appl. Sci. Manuf. 42
524 (2011) 462–470. doi:10.1016/j.compositesa.2011.01.002.

525 [37] H. Koerber, J. Xavier, P.P. Camanho, High strain rate characterisation of unidirectional
526 carbon-epoxy IM7-8552 in transverse compression and in-plane shear using digital
527 image correlation, Mech. Mater. 42 (2010) 1004–1019.
528 doi:10.1016/j.mechmat.2010.09.003.

529 [38] X. Xu, M.R. Wisnom, X. Sun, T. Rev, S.R. Hallett, Experimental determination of
530 Through-Thickness Compression (TTC) enhancement factor for Mode II fracture energy,
531 Compos. Sci. Technol. 165 (2018) 66–73. doi:10.1016/j.compscitech.2018.06.012.

532 [39] H. Cui, M. Yasaee, A.R. Melro, Dynamic inter-fibre failure of unidirectional composite
533 laminates with through-thickness reinforcement, Submitt. to Compos. Sci. Technol.
534 (2018).

535 [40] M.W. Czabaj, J.G. Ratcliffe, Comparison of intralaminar and interlaminar mode I

fracture toughnesses of a unidirectional IM7/8552 carbon/epoxy composite, Compos. Sci. Technol. 89 (2013) 15–23. doi:10.1016/j.compscitech.2013.09.008.

[41] S.A. Ponnusami, H. Cui, M. Lißner, M. Pathan, B. Erice, An integrated numerical-experimental approach to measure the dynamic Mode-I interlaminar fracture toughness of fiber composites using wedge-DCB test and cohesive zone modelling, Submitt. to Compos. Part B. (2018).

[42] M. Yasaee, G. Mohamed, A. Pellegrino, N. Petrinic, S.R. Hallett, Strain rate dependence of mode II delamination resistance in through thickness reinforced laminated composites, Int. J. Impact Eng. 107 (2017) 1–11. doi:10.1016/j.ijimpeng.2017.05.003.

[43] P. Kuhn, G. Catalanotti, J. Xavier, P.P. Camanho, H. Koerber, Fracture toughness and crack resistance curves for fiber compressive failure mode in polymer composites under high rate loading, Compos. Struct. 182 (2017) 164–175. doi:10.1016/j.compstruct.2017.09.040.

[44] K.W. Gan, M.R. Wisnom, S.R. Hallett, Effect of high through-thickness compressive stress on fibre direction tensile strength of carbon/epoxy composite laminates, Compos. Sci. Technol. 90 (2014) 1–8. doi:10.1016/j.compscitech.2013.10.010.

[45] A. Hussien, M. Moehring, C. Schwall, B. Pipes, On Compressive Response of IM7/8552 Lamina- A Theoretical & Experimental Review, (2012). doi:10.2514/6.2012-1766.

554 [46] J. Lee, C. Soutis, A study on the compressive strength of thick carbon fibre–epoxy
555 laminates, Compos. Sci. Technol. 67 (2007) 2015–2026.
556 doi:10.1016/j.compscitech.2006.12.001.

557 [47] T.K. O'Brien, A.D. Chawan, R. Krueger, I.L. Paris, Transverse tension fatigue life
558 characterization through flexure testing of composite materials, Int. J. Fatigue. 24
559 (2002) 127–145. doi:10.1016/S0142-1123(01)00104-9.

560 [48] R. Panduranga, K. Shivakumar, Mode-II total fatigue life model for unidirectional
561 IM7/8552 carbon/epoxy composite laminate, Int. J. Fatigue. 94 (2017) 97–109.
562 doi:10.1016/j.ijfatigue.2016.09.014.

563 [49] G. Catalanotti, C. Furtado, T. Scalici, G. Pitarresi, F.P. van der Meer, P.P. Camanho, The
564 effect of through-thickness compressive stress on mode II interlaminar fracture
565 toughness, Compos. Struct. 182 (2017) 153–163.
566 doi:10.1016/j.compstruct.2017.09.014.

567 [50] S.T. Pinho, P. Robinson, L. Iannucci, Fracture toughness of the tensile and compressive
568 fibre failure modes in laminated composites, Compos. Sci. Technol. 66 (2006) 2069–
569 2079. doi:10.1016/j.compscitech.2005.12.023.

570 [51] H. Körber, Mechanical Response of Advanced Composites under High Strain Rates,
571 2010.

572